OPEN ACCESS Freely available online

PLoS GENETICS

A Novel RNA-Recognition-Motif Protein Is Required for Premeiotic G_1/S-Phase Transition in Rice (*Oryza sativa* L.)

Ken-Ichi Nonomura[1,2]*, Mitsugu Eiguchi[1], Mutsuko Nakano[1], Kazuya Takashima[1], Norio Komeda[1,2], Satoshi Fukuchi[2,3], Saori Miyazaki[1,2], Akio Miyao[4], Hirohiko Hirochika[4], Nori Kurata[2,5]

1 Experimental Farm, National Institute of Genetics, Mishima, Shizuoka, Japan, **2** Department of Life Science, Graduate University for Advanced Studies (SOKENDAI), Mishima, Shizuoka, Japan, **3** Laboratory for DNA Data Analysis, National Institute of Genetics, Mishima, Shizuoka, Japan, **4** Division of Genome and Biodiversity Research, National Institute of Agrobiological Sciences, Tsukuba, Ibaraki, Japan, **5** Plant Genetics Laboratory, National Institute of Genetics, Mishima, Shizuoka, Japan

Abstract

The molecular mechanism for meiotic entry remains largely elusive in flowering plants. Only *Arabidopsis* SWI1/DYAD and maize AM1, both of which are the coiled-coil protein, are known to be required for the initiation of plant meiosis. The mechanism underlying the synchrony of male meiosis, characteristic to flowering plants, has also been unclear in the plant kingdom. In other eukaryotes, RNA-recognition-motif (RRM) proteins are known to play essential roles in germ-cell development and meiosis progression. Rice MEL2 protein discovered in this study shows partial similarity with human proline-rich RRM protein, deleted in Azoospermia-Associated Protein1 (DAZAP1), though MEL2 also possesses ankyrin repeats and a RING finger motif. Expression analyses of several cell-cycle markers revealed that, in *mel2* mutant anthers, most germ cells failed to enter premeiotic S-phase and meiosis, and a part escaped from the defect and underwent meiosis with a significant delay or continued mitotic cycles. Immunofluorescent detection revealed that T7 peptide-tagged MEL2 localized at cytoplasmic perinuclear region of germ cells during premeiotic interphase in transgenic rice plants. This study is the first report of the plant RRM protein, which is required for regulating the premeiotic G1/S-phase transition of male and female germ cells and also establishing synchrony of male meiosis. This study will contribute to elucidation of similarities and diversities in reproduction system between plants and other species.

Citation: Nonomura K-I, Eiguchi M, Nakano M, Takashima K, Komeda N, et al. (2011) A Novel RNA-Recognition-Motif Protein Is Required for Premeiotic G_1/S-Phase Transition in Rice (*Oryza sativa* L.). PLoS Genet 7(1): e1001265. doi:10.1371/journal.pgen.1001265

Editor: Li-Jia Qu, Peking University, China

Received July 22, 2010; **Accepted** December 2, 2010; **Published** January 6, 2011

Funding: This work was supported by "Genomics for Agricultural Innovation" (IPG-0016), MAFF, Japan (to K-I Nonomura); by the Grant-in-Aid for Young Scientists (S) (21678001), MEXT, Japan (to K-I Nonomura); and by the Grant-in-Aid for Scientific Research on Priority Areas (18075009), MEXT, Japan (to N Kurata). The funders had no role in study design, data collection and analysis, decision to publish, or preparation of the manuscript.

Competing Interests: The authors have declared that no competing interests exist.

* E-mail: knonomur@lab.nig.ac.jp

Introduction

The transition from mitotic to meiotic cell cycle is a central issue of reproductive development in all sexually reproducing species. Meiosis is a fundamentally different type of cell cycle from mitosis, and a pivotal event for eukaryotes to halve the chromosome number and form haploid gametes. The basic meiotic processes are evolutionarily conserved among eukaryotic species. In contrast, the signalling cascade that leads to meiosis initiation shows great diversity among species [1].

The mechanism initiating meiotic entry remains largely elusive in plants. Based on experiments using explanted pollen mother cells (PMCs) of *Trillium*, the commitment of mitotic cells to meiotic division is thought to be established during the premeiotic DNA replication (premeiotic S) or G2 phase in plants [2,3]. Only *Arabidopsis* SWITCH1 (SWI1)/DYAD and its maize homolog AMEIOTIC1 (AM1) are known to be required for the initiation of plant meiosis. Both are plant-specific coiled-coil proteins with unknown functions [4–6]. The maize *am1* mutant displays the replacement of male and female meioses by somatic mitoses, and eventually the degeneration of ameiotic meiocytes [7–9], indicating that AM1 is implicated in the decision of germ cells being directed to meiosis or mitosis. Thus, the primary function of AM1 is supposed in the premeiotic S or G2. However, immunocytological analyses revealed that AM1 diffuses inside the nucleus during premeiosis, and its localization shifts to meiotic chromosomes and pericentromeric regions during early meiosis [6], suggesting that AM1 plays a second role in progression of early meiosis. SWI1/DYAD does not seem to act directly to initiate meiosis, because it also acts in the regulation of meiotic chromosome structure and cohesion [4]. Thus, molecular mechanisms specifically underlying meiotic entry have been poorly understood in the plant kingdom.

Flowering plants have evolved an intricate network of regulatory mechanisms to ensure proper timing of the transition to flowering [10]. In addition, to achieve simultaneous fertilization within a limited season, the timing of meiotic entry is also strictly regulated. Male meiosis usually occurs in a large population of synchronously dividing cells to ensure sufficient fertility of the organisms. In plants, it is also synchronous among PMCs within an anther and among anthers within a single flower. The synchrony of male meiosis is thought to be established during premeiotic interphase. This is because the thymidine base analog, bromodeoxyuridine (BrdU), becomes incorporated synchronously into PMCs at premeiotic S [11,12], while their preceding mitoses seem to occur asynchronously. The *Arabidopsis* mutant, *tardy asynchronous meiosis* (*tam*), exhibits a phenotype of delayed and asynchronous cell divisions during male meiosis [13]. The *TAM*

Author Summary

Meiosis is a pivotal event to produce haploid spores and gametes in all sexually reproducing species and is a fundamentally different type of cell cycle from mitosis. Thus, the molecular mechanisms to switch the cell cycle from mitosis to meiosis have been studied by many researchers. In yeast and metazoans, RNA-binding proteins are known to play important roles in the post-transcriptional regulation of genes implicated in the meiotic entry and meiosis. In contrast, in the plant kingdom, the mechanisms to control the meiotic entry have largely remained elusive. In this study, we discover a novel RNA-recognition-motif (RRM) protein in rice (*Oryza sativa* L.), designated MEL2, and demonstrate that MEL2 is required for the faithful transition of germ cells from mitosis to meiotic cell cycle. Rice MEL2 shows partial similarity with human DAZAP1, which is an RRM protein and relates to Azoospermia syndrome in human, while there are critical structural differences between germline-specific RRM proteins of mammals and plants. Our findings will lead the molecular-biological studies of plant meiotic entry to the next steps and will enable a comparison of the systems of meiotic entry between animals and plants.

gene encodes an A-type cyclin that abundantly accumulates in nuclei of male meiocytes during prophase I [14], strongly suggesting that cyclins and cyclin-dependent kinases govern the synchronous progression of plant meiosis.

RNA-recognition-motif (RRM) proteins play crucial roles in the regulation of germ cell development, especially meiosis, in yeast and metazoan species. They participate in the processing, transport, localization, and translation of mRNAs [15]. In fission yeast, the RRM protein, Mei2, is necessary for the initiation of meiosis by turning off the DSR-Mmi1 system for selective elimination of over a dozen meiosis-specific transcripts during the mitotic cell cycle [16]. Deletions encompassing the human Y-linked *Deleted in azoospermia* (*DAZ*) gene cluster, encoding RRM proteins, result in a complete loss or severe reduction of germ cells in the testis. In all species examined, the expression of *DAZ*, *DAZ-like* (*DAZL*) and their homologs has been reported only in germline cells [17–19]. These RRM proteins target the adenylate-uridylate-rich element (AU-rich element; ARE) found within the 3′ untranslated region (3′UTR) of mRNAs, and control mRNA turnover rate and translation in cooperation with poly(A)-binding proteins [20,21]. Boule, the *Drosophila* ortholog of vertebrate DAZL, binds to the 3′UTR of *Twine* mRNA, which encodes a meiotic-type Cdc25 kinase, and promotes the translation of *Twine* and the premeiotic G2/M transition [18]. Mouse DAZL also binds to the 3′UTR and promotes the translation of *Sycp3* mRNA, which is a component of the synaptonemal complex (SC) [22]. In plants, redundant roles of five members of *Arabidopsis mei2*-like RNA binding proteins (AMLs) are suggested in meiotic chromosome organization [23]. The AMLs are composed of three RRMs, like fission yeast Mei2, whereas their function is presumably different from that of yeast Mei2 in meiotic entry. Therefore, in plant reproduction, no RRM protein functionally analogous to that of yeast and metazoans has been reported.

In this study, we identified a novel rice RRM protein, MEIOSIS ARRESTED AT LEPTOTENE2 (MEL2). In *mel2* anthers at early meiosis, most germ cells failed to enter the premeiotic S and meiosis, and a part escaped from the defect in the premeiotic S and underwent meiosis with a significant delay or continued mitotic cycles aberrantly. Rice MEL2 had partial similarity with human DAZ-Associated Protein1 (DAZAP1) [24]. However, MEL2 carried ankyrin repeats and the RING finger motif in addition to the RRM. This motif combination was conserved among the monocot Poaceae species, but not in dicot plants or in other organisms, despite the control of premeiotic germ-cell cycle essential for the reproduction of all eukaryotes. We will discuss structural differences and functional similarities of rice MEL2 to RRM proteins involved in the mammalian DAZ system mainly by analysis of the *mel2* mutant.

Results

mel2 mutation is caused by insertion of *Tos17* retrotransposon

Figure 1A illustrates the initiation and differentiation of rice germline cells described by Nonomura et al. [25,26]. Primordial germ cells, or archesporial cells, are initiated at the hypodermis of the stamen and the ovule primordium. In the stamen, archesporial cells generate sporogenous and parietal cells. Male sporogenous cells undergo several premeiotic mitoses, and many meiocytes are produced in each of the four locules within the anther. Parietal cells continue periclinal divisions and generate three-layered inner-anther walls, the most interior of which become tapetal cells to provide nutrients and pollen-wall materials to male meiocytes and microspores. In the ovule primordium, plural archesporial cells are initiated. Subsequently, only a single archespore which adheres to the nucellar epidermis differentiates into a single sporogenous cell, and matures into a single female meiocyte. During premeiotic maturation, both male and female meiocytes enlarge far more in cytoplasmic and nuclear volumes than somatic cells.

To elucidate the genetic network that supports early germ-cell development, we selected a seed-sterile mutant line, ND00287, in rice. The sterile segregants of this line developed normally throughout their life cycle except for seed production (Figure S1). The sterile phenotype segregated as a single recessive mutation (fertile:sterile = 141:47, chi-square (3:1) = 0.00). Microscopic observation revealed that whereas the wild type had equally sized PMCs, sterile mutants produced divergent sizes of PMCs (Figure S2), probably a result of insufficient maturation and enlargement of premeiotic cells. Gametogenesis was disrupted in both male and female organs of the mutant (Figure S1). This phenotype resembled that of the *mel1* mutant that we previously identified [26], and thus this gene was designated *MEL2*.

In anthers, the appearance of PMCs at the premeiotic interphase was unlikely to have been affected by the *mel2* mutation, except callose accumulation around the cells was lacking in the mutant (Figure 1B, 1G). Callose is one of the cell wall component, and plays a vital role in the process of pollen development [27]. Interestingly, in *mel2-1* mutant anthers, 0.69% of premeiotic germ cells (n = 291) underwent the mitotic metaphase, whereas no PMCs did in the wild type (n = 311) (Figure 1B, 1G). While the wild-type PMCs entered and underwent normal meiosis, the mutant PMCs were drastically hypervacuolated (Figure 1C, 1H). In the wild type, haploid microspores were released from tetrads after the completion of meiosis (Figure 1D). In contrast, highly vacuolated mutant PMCs failed to produce tetrads and microspores (Figure 1I). In addition to a failure in meiosis, tapetal cells also became aberrantly vacuolated and hypertrophic (Figure 1I). Highly vacuolated PMCs underwent apoptotic DNA fragmentation, revealed by the TdT-mediated dUTP-biotin nick end labeling (TUNEL) method (Figure 1E, 1J). Aberrantly hypertrophic tapetal cells also caused apoptosis at a step earlier than the programmed cell death (PCD) in normal process of tapetal development (Figure 1E, 1J). A serious

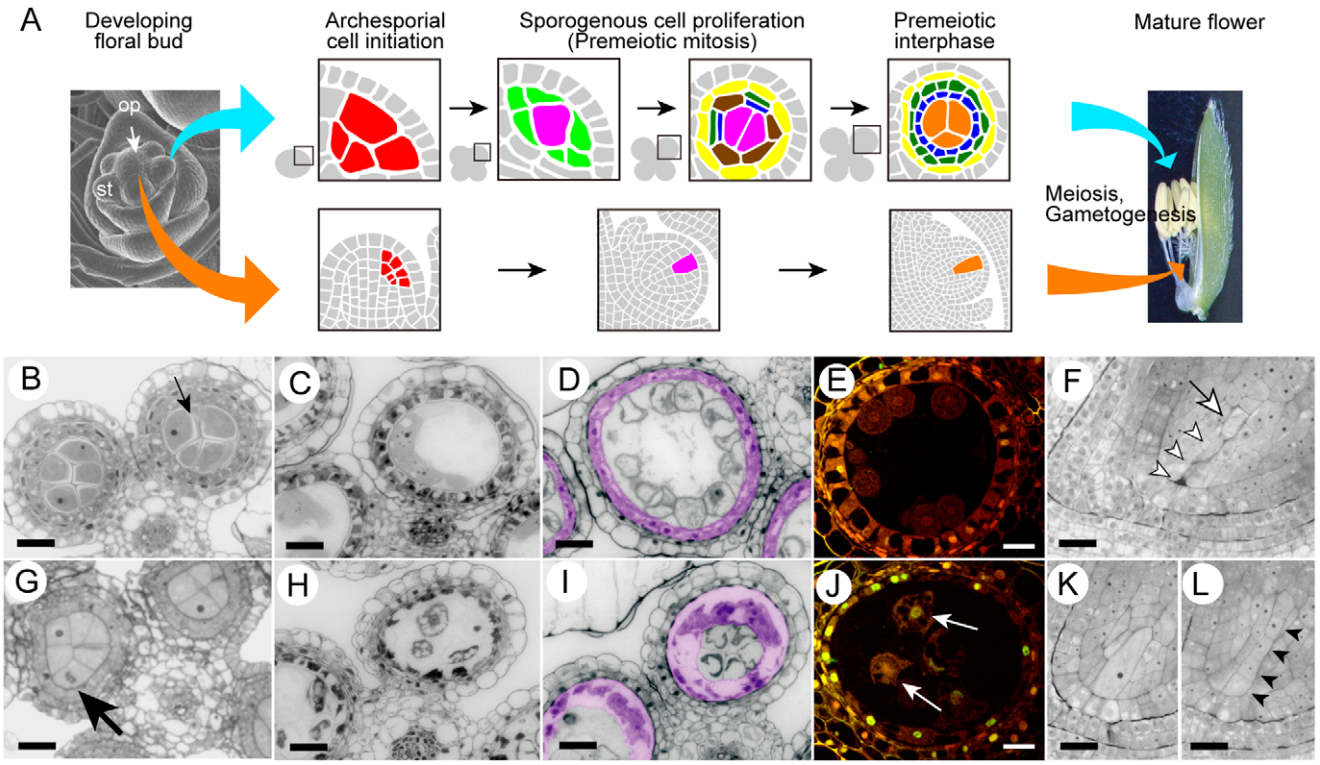

Figure 1. Developmental aberration of germline and nursery cells in the *mel2* mutant. (A) A schematic illustration of the germline cell development in the anther and ovule in rice. Red-colored cells indicate the archesporial cells; magenta, sporogenous cells; light green, primary parietal cells; yellow, endothecium; brown, secondary parietal cells; dark green, middle layer cells; blue, tapetal cells; mandarin, meiocytes at premeiotic interphase. (B–L) Plastic sections of wild-type (B–F) and *mel2* (G–L) reproductive organs during sporogenesis. (B, G) Premeiotic interphase. The callose accumulation among PMCs (a small arrow) was absent in the mutant. A large arrow indicates asynchronous, aberrant mitosis of the PMC. (C, H) Meiotic I prophase (diakinesis). (D, I) Post-meiotic microspore stage. Tapetal cells were pseudo-colored in magenta. (E, J) TUNEL assay. White arrows indicate TUNEL signals representing apoptotic DNA fragmentation found in nuclei of disrupted PMCs. (F, K, L) Ovules at post-meiosis. Three of tetrad spores (open arrowheads) were degenerated, and a single megaspore (an open arrow) underwent megagametogenesis after the completion of wild-type meiosis, whereas meiosis progression was stagnant at various steps in the mutant (K, L). Closed arrowheads indicate an equal size of tetrad spores. Bars, 10 μm.
doi:10.1371/journal.pgen.1001265.g001

defect in meiosis progression was also observed in the megaspore mother cell (MMC), the female meiocyte. When three of the tetrad spores had been degraded in the wild-type ovule (Figure 1F), the mutant MMC was still before meiotic cell division (Figure 1K) or the tetrad before degradation of three spores (Figure 1L). Surprisingly, in contrast to PMCs, no conspicuous vacuolation was observed in the MMC.

Though the ultrastructure of PMCs was also observed, no remarkable difference was observed between the wild type and *mel2* mutant at the premeiotic interphase (data not shown). However, at the meiotic prophase I, *mel2* PMCs were hypervacuolated, but not in the wild-type PMCs, and in addition, mitochondria were enlarged in *mel2* PMCs extremely more than those in wild types (Figure S3). The formation of megamitochondria is known to precede apoptosis in the cells treated with various free radical-generating chemicals [28]. Thus, the ultrastructural analysis also suggested that the *mel2* PMCs were directed to apoptosis.

Southern blot analysis of the ND00287 population revealed that the *Tos17* insertion showed complete genetic linkage with the seed-sterile phenotype (Figure S4). This insertion tagged the gene locus, *Os12g0572800*, in Rice Annotation Project Database build4 (RAP-DB, http://rapdb.dna.affrc.go.jp/). When the 10-kbp wild-type genomic fragment including this locus was introduced into *mel2* homozygous plants, the transformants recovered fertility (Figure S4). Furthermore, NE04525 carrying another allelic *Tos17* insertion in this locus (*mel2-2*) exhibited the same *mel2* phenotype (data not shown). Thus, we concluded that the *Tos17* insertion into *Os12g0572800* caused the *mel2* mutation.

MEL2 gene encodes novel protein with RNA-recognition motif

Full-length *MEL2* cDNA was obtained from young panicles, including germ cells at developmental stages earlier than meiosis, by 5′-rapid amplification of cDNA ends (RACE) technology. To determine the transcriptional start site of *MEL2* mRNA, three rounds of 5′RACE were performed. Four independent RACE libraries were produced by a gene-specific antisense primer nearest to the 5′ end (Figure S4B), and 16 of 17 RACE sequences terminated at the same 5′-endpoint. The putative start site predicted in this study mapped to 254 bp upstream from the location annotated in the RAP-DB. The *MEL2* gene was composed of 14 exons and 13 introns (Figure S4). The *MEL2* cDNA encoded a novel protein of 1,160 amino-acid residues (aa) of previously unknown function (DDBJ, AB522964). An online motif search revealed three conserved domains in the deduced MEL2 sequence: ankyrin repeats (ANKs, PF00023), an RNA recognition motif (RRM, PF00076), and a C3HC4-type RING finger motif (RING, PF00097) (Figure 2, Figure S5). An N-myristoylation consensus sequence, which allows protein binding

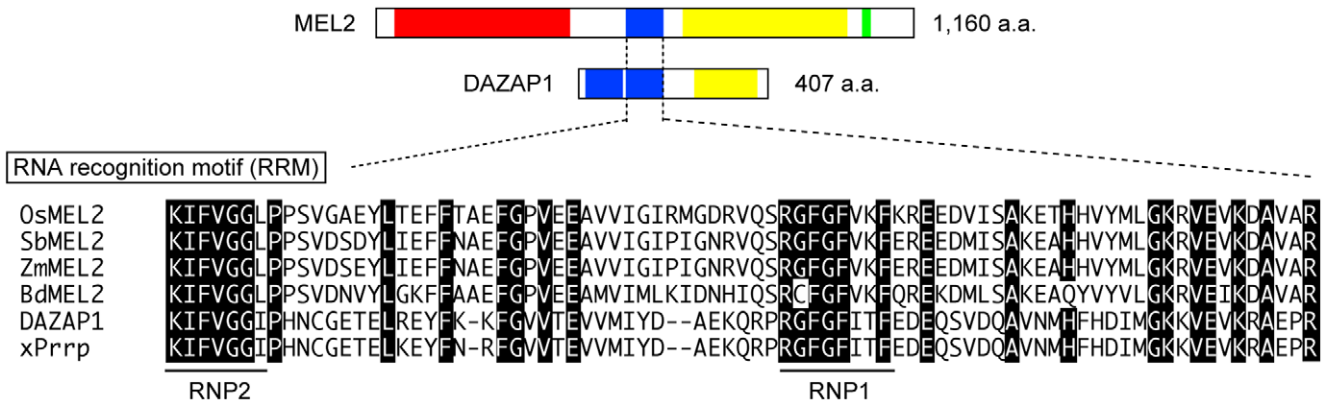

Figure 2. Rice MEL2 is the RRM protein partially homologous to human DAZAP1. The single RRM of MEL2 is followed by a proline-rich sequence (yellow) like human DAZAP1, whereas DAZAP1 carries a doublet of RRMs. MEL2 possesses three additional motifs; The N-myristoylation target, the ankyrin repeats (red), and the RING finger motif (green). The peptide sequence of each motif is aligned and compared with known consensus sequence and/or sequences of other organisms, in which identical amino-acid residues are highlighted. Os, rice (*Oryza sativa*); Sb, *Sorghum bicolor*; Zm, *Zea mays*; Bd, *Brachypodium distachyon*; DAZAP1, huma DAZAP1 (UniProt/Swiss-Prot: Q96EP5); xPrrp, *Xenopus* Proline-rice RNA binding Protein (Vg1) (Q98SJ2).
doi:10.1371/journal.pgen.1001265.g002

to the plasma membrane or other intracellular membranes in eukaryotic cells [29], was found at the N-terminal end.

ANKs are implicated in protein-protein interactions [30]. Rice MEL2 contained 10 imperfect and tandemly aligned copies of ANKs (Figure S5). The RRM consisted of 80–90 aa with two highly conserved short motifs, an RNP1 octamer and an RNP2 hexamer, which are found in numerous proteins involved in post-transcriptional processes [31–33]. MEL2 contained a single RRM that conserved both RNP1 and RNP2 sequences (Figure 2). The MEL2 peptide sequence excluding the ANKs (451 aa to the end) showed similarity to human DAZAP1 in a BLASTp search (Score = 62.4 bits; E-value = 1e−07) [34]. DAZAP1 contains two RRMs at the N-terminus and a proline-rich domain at the C-terminus [24]. The C-terminal half of rice MEL2 was also rich in proline residues (615 to 1,042 aa, Figure 2).

The rice MEL2 sequence was evolutionarily conserved among Poaceae species; *Sorghum bicolor*, *Brachypodium distachyon*, and *Zea mays* (Figure 2, Figure S6). The *Sorghum* locus *Sb08g018890* and the *Brachypodium* locus *Bd04g03890* encoded putative proteins of 1,083 and 1,076 aa, 77.1% (813/1,055 aa) and 75.5% (791/1,048 aa) identical to rice MEL2, respectively. The *Zea* locus *AC208308.3_FGP002* showed high conservation of the RRM and RING, but not the ANK, probably because the sequence information was incomplete in maize genome. The RRM followed by the proline-rich sequence was also conserved in these three species. No proteins carrying a combination of the three domains, ANK, RRM and RING, were found within the genome of the dicot model plant *Arabidopsis thaliana*, nor did we detect any proteins with the three-domain combination in genome information from 787 species included in the Archaea, Bacteria, Eukaryota and Viruses by *in silico* searches of the GTOP web database [35,36]. Thus, we concluded that the motif combination found in rice MEL2 is unique to Poaceae or monocot plants.

The rice genome contained another predicted gene locus, *Os12g0587100*, similar to *MEL2* (Figure S7). *Os12g0587100* was located about 0.9-Mbp from the *MEL2* locus toward the telomere side on the long arm of chromosome 12. Putative coding sequences of this locus were highly homologous to those of the *MEL2* gene, while the homology was lost in the exon 12 and the following exons.

MEL2 mRNA is expressed in germline and tapetal cells before meiosis

The spatiotemporal expression of *MEL2* mRNA was examined by reverse-transcription PCR (RT-PCR) and *in situ* hybridization techniques. Based on the results of RT-PCR, the *MEL2* mRNA was expressed mainly in young panicles and flowers (Figure S8). *In situ* hybridization revealed that the *MEL2* expression was initiated in male and female archesporial cells at the hypodermis of stamen and ovule primordia (Figure 3A–3C). In the ovule, the *MEL2* mRNA was expressed in multiple archesporial cells during early stages (Figure 3B, 3C), and subsequently in a single sporogenous cell (Figure 3D, 3E). In the stamen, strong *MEL2* signals were detected in sporogenous cells (Figure 3D, 3F), and in addition, faint signals were also observed in parietal cells, which generate tapetal cells (Figure 3F). The *MEL2* signal disappeared before meiosis in both male and female organs (Figure 3G). Thus, we concluded that the *MEL2* gene was expressed in male and female germline cells from their initiation to meiosis, and weakly in male nursery cells including tapetal cells. The *mel2-1* mutant flowers transcribed only aberrant types of *MEL2* mRNA, which contained a 4.0-kbp *Tos17* insertion within the seventh exon (Figure S9). This insertion was predicted to cause an in-frame stop codon at the 5′-end of the insert, and to result in a truncated form of MEL2 protein without the RRM and RING, if any was translated. Thus we concluded that the *mel2-1* was a null allele.

The *MEL2*-like *Os12g0587100* locus was also transcribed, and its transcripts were detected in young panicles and flowers (Figure S8). Sequencing the RT-PCR product revealed that the *MEL2*-like cDNA included many nucleotide polymorphisms against *MEL2* cDNA, which could induce a shift in reading frame that would result in lack of RRM and RING motifs (data not shown). Therefore, the *MEL2*-like locus was considered to be a pseudo-gene.

MEL2 function is excluded from premeiotic mitosis

If MEL2 had functioned during premeiotic mitosis prior to premeiotic interphase, the number of PMCs would be decreased in *mel2-1* mutant anthers. However, it was not different significantly between PMC numbers in the wild type (103.7±15.3 per anther locule; average of three anthers) and the mutant (97.0±6.6). In addition, no remarkable aberration in the

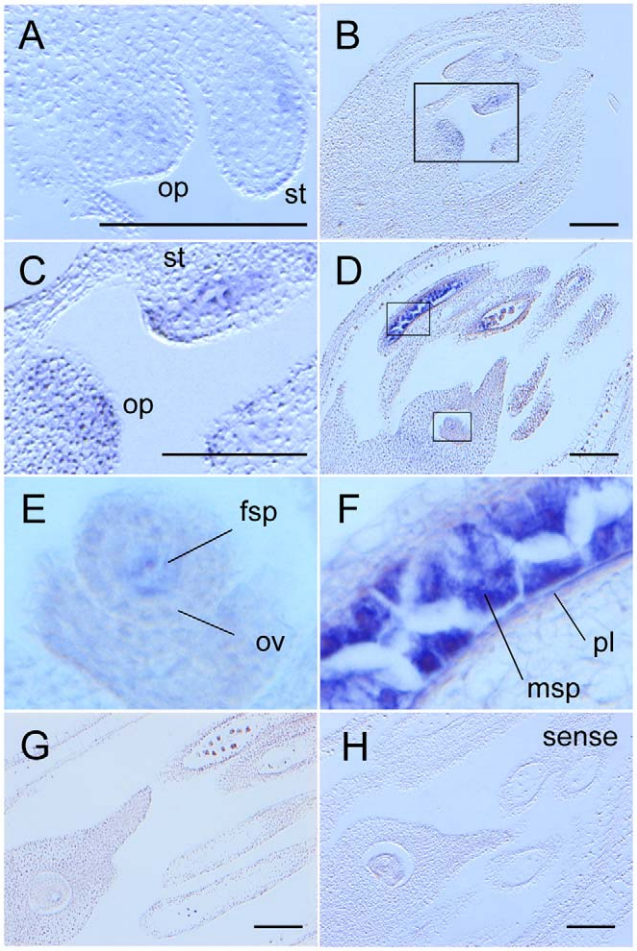

Figure 3. *MEL2* mRNA was expressed in male and female germline and parietal cells before meiosis. (A) The initiation stage of archesporial cells. A faint *MEL2* signal (blue) appeared at hypodermis of stamen (st) and ovule primordium (op). (B) Early premeiotic mitosis stage. (C) A magnified image of (B). In op, plural hypodermal cells expressed *MEL2*. (D) The late premeiotic mitosis stage. (E, F) Magnified images of (D). The faint *MEL2* signal was observed in female sporogenous cell (fsp) (E). Microsporocytes (msp) strongly expressed *MEL2*, and parietal layer cells (pl) adhered to msp were also stained (F). (G) No MEL2 signal was detected in and after meiosis. (H) A sense probe as a negative control gave no signal in the same stage with (D). Bars, 100 μm.
doi:10.1371/journal.pgen.1001265.g003

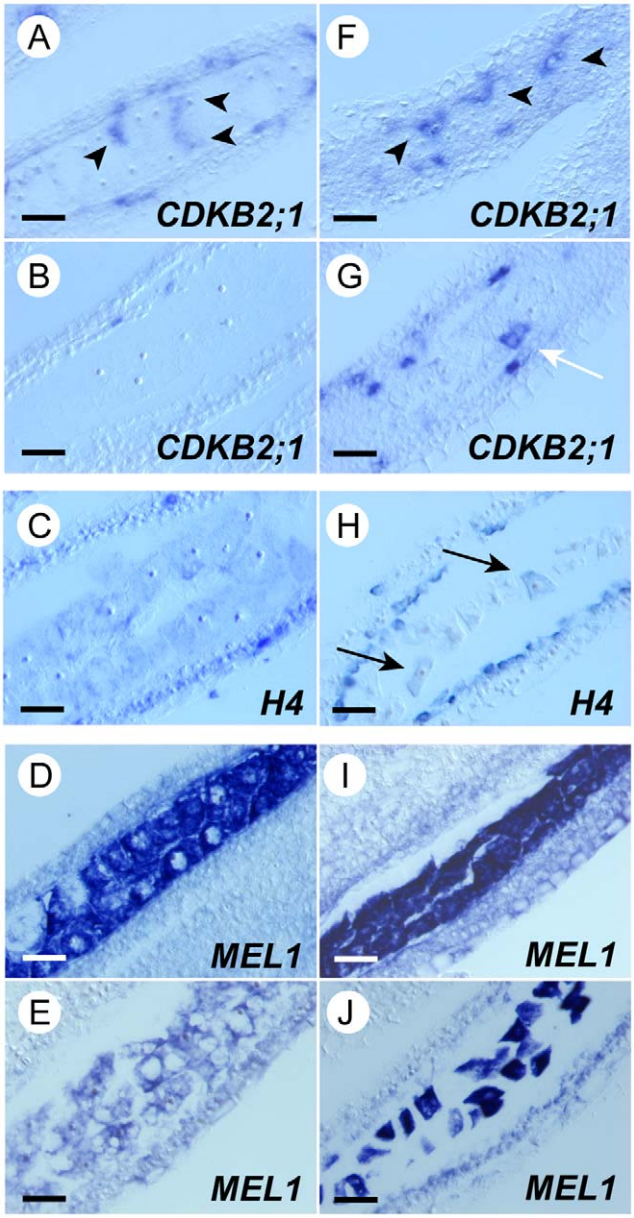

Figure 4. Synchronous initiation of premeiotic S was disrupted among *mel2* germ cells. The longitudinal sections of wild-type (A–E), and *mel2* anthers (F–J). (A, F) During sporogenous cells undergoing premeiotic mitosis, *CDKB2;1* mRNA, the marker of G2/M transition, was expressed in patches in both wild-type and *mel2* anthers (arrowheads). (B, G) During premeiotic interphase, *CDKB2;1* expression was synchronously suppressed in wild-type anthers (B), whereas it was still in patches in *mel2* anthers (G). (C, H) During premeiotic S or the onset of meiosis I, histone *H4* mRNA, the marker of S-phase, was expressed simultaneously (C), while only a few germ cells expressed the *H4* (H). (D, I) During sporogenous cells undergoing premeiotic mitosis, *MEL1* mRNA, the marker of archesporial and sporogenous cells, was strongly expressed in sporogenous cells. (E, J) In early meiosis I, *MEL1* expression was drastically downregulated in wild-type anthers (E), whereas kept at a higher level in *mel2* anthers (J). Bars, 20 μm.
doi:10.1371/journal.pgen.1001265.g004

morphology of reproductive tissues and germ cells was observed in the *mel2* anthers during the premeiotic-mitosis stage (Figure 1G). These observations indicate that MEL2 function was excluded from the premeiotic-mitosis stage of male germ cells.

MEL2 is required for germ cells to enter the premeiotic S-phase

To investigate whether the *mel2* germ cells could pass through the premeiotic interphase normally, we examined the expression profile of several cell cycle-related genes in *mel2* mutant anthers. The rice histone *H4* mRNA is abundantly expressed during S-phase, and *CDKB2;1* (*cdc2Os3*) is enriched during G2/M transition, but is less abundant or absent during S-phase in rice mitosis [37]. During premeiotic mitosis, *CDKB2;1* was expressed in patches in both wild-type and *mel2-1* anthers (Figure 4A, 4F), indicating that premeiotic germline mitoses occur asynchronously in the wild type and are unaffected by the *mel2* mutation. At the boundary of premeiotic interphase and meiosis, no expression of *CDKB2;1* mRNA was detected in the wild type (Figure 4B), indicating that the cells entered synchronously into premeiotic S, whereas *CDKB2;1* was still expressed in patches in the *mel2* anther

(Figure 4G). At the same stage, *H4* mRNA was expressed in all PMCs of wild-type anthers (Figure 4C). In contrast, in *mel2* anthers, only a few PMCs exhibited *H4* signal (Figure 4H). The asynchronous expression of *CDKB2;1* and *H4* was observed in anthers of three independent *mel2* plants at the stages that the wild type underwent early meiosis. The *MEL1* gene, which encodes an Argonaute family protein, is expressed exclusively in germline cells before meiosis [26]. In the wild type, *MEL1* mRNA was strongly detected in sporogenous cells undergoing premeiotic mitosis (Figure 4D), and was rapidly downregulated during premeiotic interphase (Figure 4E). Premeiotic *mel2* sporogenous cells also expressed *MEL1*, same as wild-type cells (Figure 4I). However, the expression continued aberrantly in early meiotic stages (Figure 4J).

Next, we performed the BrdU incorporation experiment for the premeiotic athers. In the wild type, ten of 31 flowers at the premeiotic interphase had anthers in which PMCs incorporated BrdU into their nuclei synchronously, whereas the most *mel2* flowers had anthers that showed asynchronous incorporation of BrdU into the PMC nuclei (Figure 5A). In most of *mel2* anthers, only 20% of PMCs incorporated BrdU simultaneously (Figure 5B, 5C).

These results clearly indicate that MEL2 plays essential roles in the decision for germ cells to enter the premeiotic S-phase.

mel2 germ cells failed to undergo normal meiosis

Next, we examined whether the *mel2* mutant PMCs were able to enter meiosis. Telomere clustering or a bouquet structure, a typical feature of zygotene meiocytes in maize [38], was observed in four of 10 wild-type meiocytes, whereas no bouquet was observed in any of 31 *mel2-1* meiocytes (Figure S10). In wild-type soma and premeiotic meiocytes, centromeres and telomeres were arranged in peripheral and interior regions of the nucleus, respectively, and their positions were inverted during meiotic entry. However, *mel2* PMCs at early zygotene lacked this inversion, retaining a soma-like centromere arrangement (Figure S10). Further, we performed immunofluorescent detection of rice meiotic proteins PAIR2 and ZEP1. PAIR2 transiently associates with meiotic chromosome axes and is required for SC establishment [39]. ZEP1 is a component of the transverse filament of SC [40]. Both genes were transcribed normally even in *mel2* flowers (Figure S8). In wild-type meiocytes at early zygotene, PAIR2 associates along meiotic chromosome axes, and filamentous ZEP1 signals begin to elongate between homologous axes (n = 101) (Figure 6A). In contrast, in all *mel2* meiocytes (n = 118) at early zygotene, neither PAIR2 nor ZEP1 was detected on chromosomes (Figure 6B). These observations indicate that *mel2* meiocytes fail to enter meiosis when the wild type undergoes early zygotene.

At late zygotene in wild-type meiocytes, ZEP1 stretches extended overall meiotic chromosomes and most PAIR2 proteins had been removed from the axes, indicating the completion of homologous synapsis (Figure 6C). In *mel2* meiocytes, 79.7% of meiocytes (n = 64) exhibited faint or abnormally dotted signals of PAIR2 in nuclei (Figure 6D). All these meiocytes showed a soma-like centromere arrangement. However, the remaining 20.3% showed an early zygotene-like, filamentous appearance of PAIR2 and a meiotic centromere arrangement (Figure 6E), whereas ZEP1 proteins, which failed to be loaded on homologous axes, accumulated aberrantly in the cytoplasm. It was impossible to observe whether the mutant PMCs emanating filamentous PAIR2 signals underwent subsequent meiotic steps, because of significant cell disruption due to hypervacuolation (Figure 1I) and apoptosis (Figure 1J).

These results strongly suggest that in *mel2* mutant, most of male germ cells which show the defect in the premeiotic G1/S transition result in the lack of meiosis, even though meiotic genes have been normally expressed. The 20% cells could escape from the defect in the transition and enter early meiotic stages, but extremely later than usual, and yet they failed to establish the SC between homologous chromosome pairs until the apoptosis.

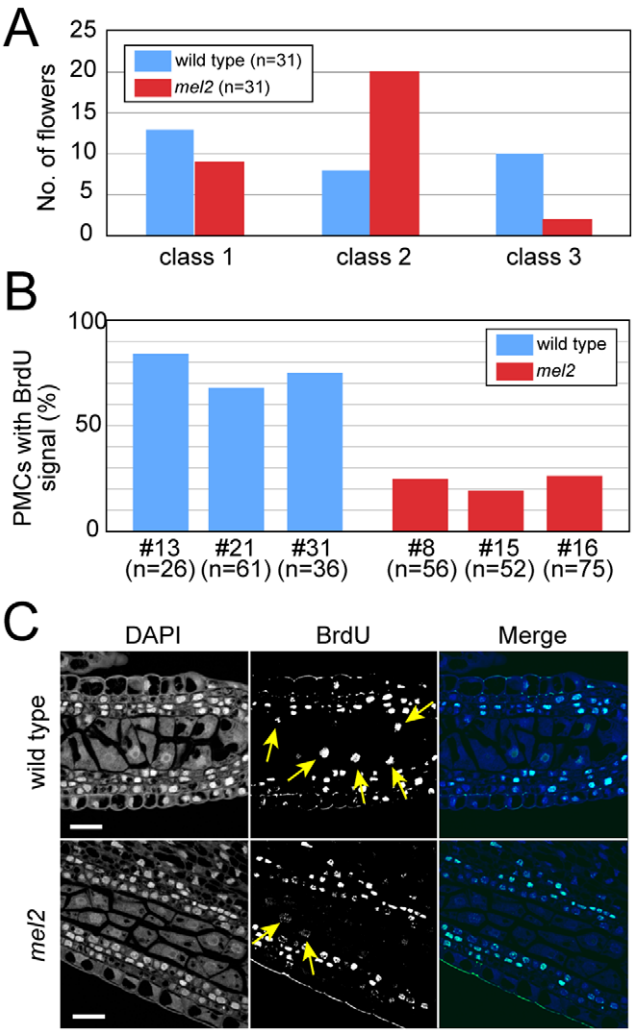

Figure 5. The *mel2* mutation abolished synchronous incorporation of bromodeoxyuridine (BrdU) in an anther at premeiotic interphase. (A) The number of flowers with pollen mother cells (PMCs) emanating the BrdU signal was counted. Flowers at premeiotic interphase (with about 0.4-mm anthers) were provided for the BrdU incorporation experiment. Flowers emanating the BrdU signal in 0%, less than 50%, and more than 50% of PMCs were classified into classes 1, 2 and 3, respectively. (B) A percentage of BrdU-incorporated PMCs in an anther was measured in three plants (#: the plant number) each of the wild type and *mel2* mutant. (C) Longitudinal sections of BrdU-incorporated anthers at premeiotic interphase. The wild-type anthers frequently contained a lot of PMCs emanating the intense BrdU signal in an anther locule (top), while the *mel2* anthers contained a few (bottom). Yellow arrows indicate the nuclei emanating the BrdU signal. Bars, 20 μm.
doi:10.1371/journal.pgen.1001265.g005

MEL2 protein localizes to perinucleus of premeiotic meiocytes

The seed-sterile phenotype of *mel2* homozygous plants was rescued by introducing transgenes expressing the MEL2 protein with a T7-peptide tag at the C-terminus (C-tagged) (Figure S11), indicating that this recombinant protein is functional *in vivo*.

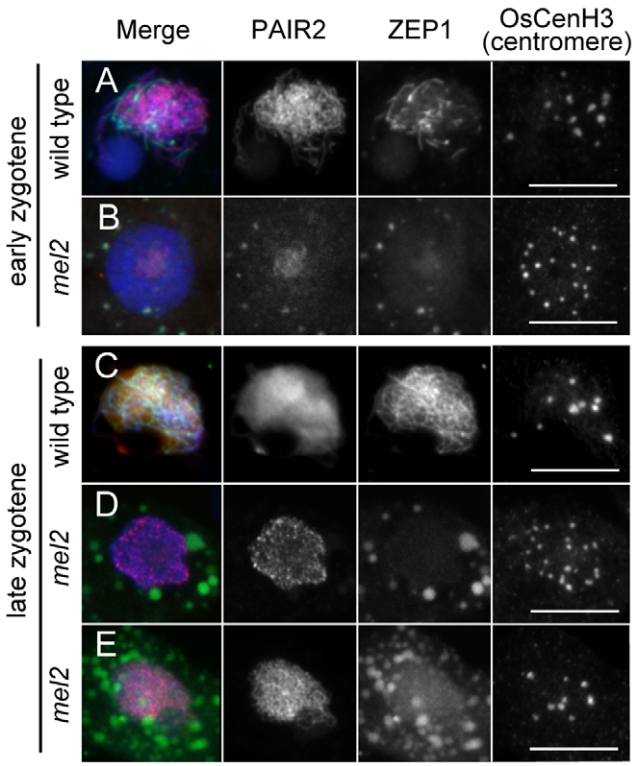

Figure 6. The absence of homologous chromosome synapsis in *mel2* mutant anthers. Chromosomes were counter-stained with DAPI (blue). (A, B) Meiocyte nuclei at early zygotene in the wild type (A) and *mel2* mutant (B). (C, D, E) Meiocyte nuclei at late zygotene in the wild type (C) and *mel2* mutant (D, E). In 79.7% of *mel2* meiocytes, PAIR2 and ZEP1 were aberrantly accumulated, and the arrangement of OsCenH3 foci was soma-like (D). The remaining 20.3% of the meiocyte nuclei exhibited filamentous PAIR2 signals, comparable to those in wild-type early zygotene, and the centromere arrangement became meiotic (E). Bars, 10 μm.
doi:10.1371/journal.pgen.1001265.g006

Unfortunately, we failed to obtain any clear signals of the T7-tagged protein in western blotting (data not shown), probably because of the low level and spatiotemporal limitations of its expression. However, indirect immunofluorescence enabled to visualize the subcellular protein localization. In wild-type PMCs undergoing premeiotic mitosis, a faint signal was observed in the cytoplasm (Figure 7A). In premeiotic interphase, signals were found in the cytoplasm, especially concentrated at the perinuclear region (Figure 7B). By early meiosis I, MEL2 had been released to the cytoplasm of PMCs, and in turn, a faint signal appeared at the perinuclear cytoplasmic region of the inner anther-wall cells, including tapetal cells (Figure 7C). MEL2 signals finally disappeared at post-meiotic stages of PMCs and anther-wall cells (data not shown). This localization was observed in seven of eight anthers from two independent plants (C6#2, C9#2 in Figure S11). The C-tagged MEL2 signal was excluded from the nucleoplasm in any of these stages. In transgenic plants expressing N-tagged MEL2 protein, the immunofluorescent signal diffused over all the cytoplasm in premeiotic PMCs (Figure 7D). N-myristoylation is a post-transcriptional protein modification, in which myristic acid is covalently attached to an N-terminal glycine residue, exposed during cotranslational N-terminal methionine removal by N-myristoyltransferase [41]. Thus, the immunofluorescence of N-tagged MEL2 may represent the first methionine residue with the T7 tag that had been removed and diffused throughout the cytoplasm.

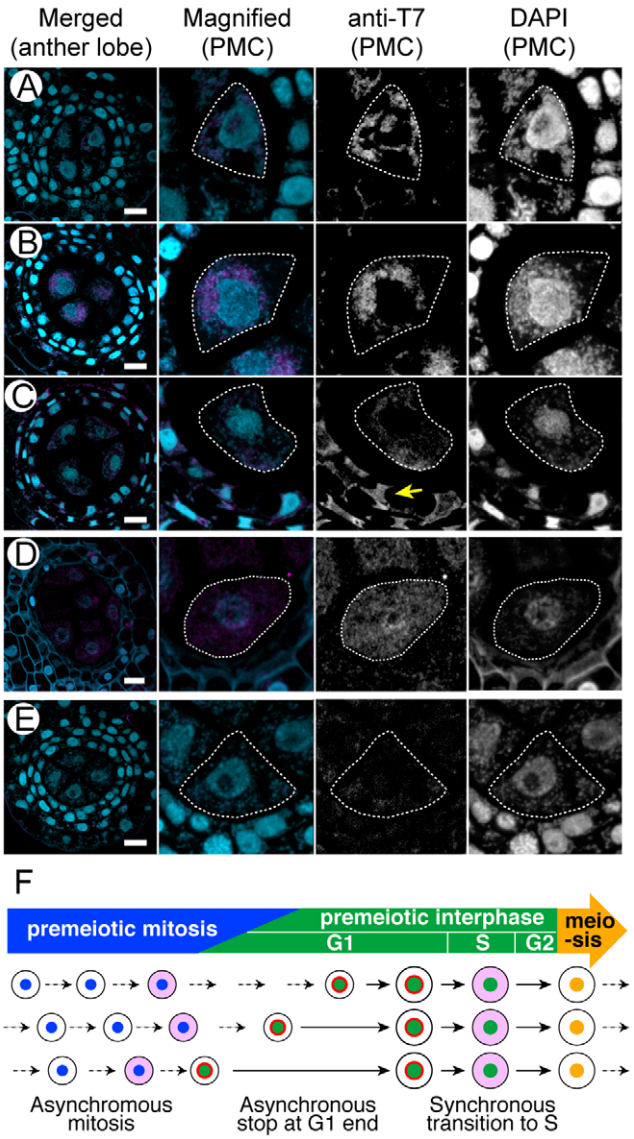

Figure 7. Subcellular localization of the T7 peptide-tagged MEL2 in anthers of transgenic rice plants. Plastic cross-sections of transgenic anthers were counter-stained with DAPI (blue). Pollen mother cells (PMCs) were outlined with the broken lines. (A–C) Transgenic anthers expressing the C-tagged MEL2 (magenta). (A) Premeiotic mitosis stage. (B) Premeiotic interphase. A yellow arrow indicates the anti-T7 signals observed in the cytoplasm of tapetal cells. (C) Early meiosis I. (D) A transgenic anther expressing the N-tagged MEL2 (magenta) in premeiotic interphase. (E) An anther in premeiotic interphase transformed with the empty vector as a negative control. Bars, 10 μm. (F) The summary of MEL2 subcellular localization observed in (A–C). Smaller circles within larger ones indicate nuclei of germ cells. The pink and red indicate the subcellular localization of MEL2 at the cytoplasm and the perinuclear region, respectively. Broken and solid arrows indicate the cell division cycle and the cell maturation without the division.
doi:10.1371/journal.pgen.1001265.g007

Discussion

MEL2 plays an essential role in premeiotic cell-cycle control

This study provides the first evidence that the novel RRM-containing protein plays essential roles in meiotic entry in rice. In the *mel2* mutant, the progression of male and female meioses was significantly affected, and the male meiocyte and tapetal cells were hypervacuolated and directed to apoptosis (Figure 1, Figure S3).

The *mel2* mutation disturbed the most germ cells to transit into the premeiotic S-phase in anthers (Figure 4 and Figure 5). However, twenty percents of the cells could enter the S-phase (Figure 5B) and undergo meiotic processes in which chromosomes showed a typical appearance of early zygotene (Figure 6), while the wild-type cells underwent late zygotene. In these cells, neither precocious separation of sister chromatids nor sister centromeres was observed. This result indicates that the MEL2 function might be excluded from the regulation of meiotic chromosome structure and cohesion, different from the function of *Arabidopsis* SWI1/DYAD. Thus, the role of rice MEL2 could be specified in the premeiotic cell-cycle control.

The MEL2 function in premeiotic interphase will be tangible in comparison with that of maize AM1, the coiled-coil protein also controlling meiotic entry. AM1 is implicated in the decision of germ cells being directed to meiosis or mitosis [6]. Interestingly, in the *am1* mutant, ameiotic mitoses replacing meioses occur synchronously [7], indicating that the synchrony of male meiosis is genetically separable from the meiosis commitment, and also that the AM1 function can be allocated into the meiosis commitment following the establishment of synchrony. In contrast, in the rice *mel2* mutant, most of male germ cells could not enter the premeiotic S and lost the synchrony (Figure 4 and Figure 5). Thus, it is strongly suggested that the MEL2 function precedes the establishment of synchrony, the meiosis commitment and the function of maize AM1. The ameiotic mitoses also occurred in the *mel2* anther, but only in a small amount of male germ cells (Figure 1G), probably representing that some of the PMCs would return to the mitotic cell cycle before the meiosis commitment. Taken together, we conclude that MEL2 plays an essential role in the premeiotic G1/S-phase transition in rice.

Pawlowski et al. [6] proposed the existence of a novel checkpoint system monitoring faithful transition of leptotene to zygotene based on the degeneration phenotype of *am1* mutant PMCs. Our results may support this proposal in rice. The *mel2* mutant PMCs initiated hypervacuolation and apoptosis simultaneously when wild-type PMCs underwent early meiosis (Figure 1). This degeneration of meiocytes would be an indirect effect of the *mel2* mutation, because it was never observed in the *mel2* MMCs (Figure 1K, 1L). In yeast and metazoans, a system referred to as pachytene checkpoint monitors for defects in homologous recombination and synapsis, and meiocytes arrested in pachytene will eventually be eliminated [42]. In contrast, plants are thought to lack the typical meiotic checkpoint [43]. This consideration has been based on most plant meiotic mutants being able to complete meiosis, while fragmentation or nondisjunction of chromosomes takes place. However, most plant materials examined so far are thought to have been mutated in meiotic machinery, but not in premeiotic events. In turn, the function of maize AM1 and rice MEL2 is supposed in premeiotic events, in contrast to the meiotic mutants previously reported in plants.

In this study, we mainly focus on male meiosis, because in rice, it is easier to be observed than female meiosis. However, the *mel2* mutation also affected the progression of female meiosis (Figure 1K, 1L). The fundamental role of MEL2 might be in the initiation of premeiotic G1/S transition in the appropriate timing in both male and female cells.

Similarities and differences of rice MEL2 to mammalian DAZ-related proteins

The central region of MEL2 protein resembles human DAZAP1, whereas MEL2 possesses a single RRM, in contrast to the doublet in DAZAP1 (Figure 2). DAZAP1 is a member of the proline-rich RNA-binding proteins (PRRPs) [24], and also of the heterogeneous nuclear ribonuclear proteins (hnRNPs), known to bind to newly synthesized RNA transcripts and participate in their processing and export [44]. A role of human DAZAP1 in transcription is suggested by its specific exclusion from the transcriptionally inert XY body in the nuclei of pachytene spermatocytes, and a requirement for active transcription for its nuclear localization [45,46]. Mouse DAZAP1 is also detected in the nucleus of pachytene spermatocyte, and its localization dramatically shifts from the nucleus to the cytoplasm during the maturation of spermatids [45,47]. In male *dazap1* mutant mice, spermatogenesis is arrested before the first meiotic division, and the cells are directed to apoptosis, whereas the female has largely normal oogenesis [48].

Human DAZAP1 is an interacting counterpart of DAZ and DAZL proteins [24]. DAZ, DAZL and BOULE are able to form an RNA-protein complex with another RNA-binding protein, PUM2, while they may function in distinct molecular complexes during germ cell development [49,50]. In addition, yeast two-hybrid screening of testis proteins revealed that human DAZ interacts with DZIP3 (DAZ-interacting protein3)/hRUL138 [49], which has the potential for RNA binding and RING E3-ubiquitin ligase. DZIP3/hRUL138 is expressed ubiquitously in various tissues, and is localized to certain cytoplasmic structures, especially perinuclear regions, but excluded from the nucleoplasm [51]. Thus, in the mammalian system, RNA-binding proteins, such as DAZ, DAZL, DAZAP1 and PUM2, first associate with the target mRNA precursors in the nucleus of germline cells. They export the mature targets to the cytoplasm, form a complex with ubiquitously expressed cytoplasmic proteins, such as DZIP3/hRUL138, on the cytoplasmic nuclear membrane or endoplasmic reticulum, and regulate the translation of target mRNAs.

Rice MEL2 localized the perinuclear region, but it was excluded from the nucleoplasm of germ cells, distinct from mammalian DAZ families (Figure 7). We hypothesize that MEL2 may be a hybrid form of a DAZAP1-like protein and a DAZ-interacting E3 ligase, such as DZIP3/hRUL138, and may have evolved to acquire a germline-specific function in ancestral monocots. This idea raises the possibility that RING E3 ligase-dependent ubiquitination is required for germline development commonly in eukaryotic species. It is also suggested that unknown DAZ-family proteins that transport the target mRNAs from the nucleoplasm to the cytoplasm exist in plant germline cells.

The *Arabidopsis* locus *At5g57740* or *XBAT32* encodes a MEL2-like protein composed of ANK and RING motifs at the N- and C-termini, respectively, but not of RRM, and it promotes lateral root formation by inhibiting ethylene biosynthesis [52,53]. XBAT32 is expressed ubiquitously in various *Arabidopsis* tissues, but most abundantly in anthers. We hypothesized that domain-shuffling events occurred between an RRM protein and a XBAT32-like protein required for meiotic entry in ancestral monocots after the monocot-dicot divergence around 200 million years ago [54].

Synchrony of male meioses closely relates to premeiotic G1/S-phase transition in plants

In the *mel2* mutant, synchronous progression of premeiotic S-phase was completely disrupted (Figure 4 and Figure 5). This *mel2* phenotype indicated that the genetic system controlling the premeiotic G1/S-phase transition would closely relate to the system terminating the premeiotic mitosis and establishing the synchronous progression of premeiotic- and meiotic-cell cycles in the rice anther. Figure 7F summarizes a transition of subcellular localization of MEL2 protein. It is plausible by analogy with the mammalian DAZ system that the perinuclear localization of MEL2 functions in the translational inhibition of some cell-cycle

related gene(s), cooperating with the perinuclear translational machineries. MEL2 may temporarily arrest the progression of asynchronous germ-cell cycles at premeiotic G1 end or the onset of S-phase at the perinuclear region, and the synchronous release of MEL2 to the cytoplasm allows the cells to enter premeiotic S-phase synchronously within an anther. The identification of binding substrates of MEL2 will contribute to evidence this hypothesis.

According to this idea, unknown signalling factor(s) should be hypothesized to mediate cell-cell communication and promote the synchronous release of MEL2 from the perinucleus. During premeiotic interphase and early meiosis, it is known that male meiocytes form a single coenocyte in an anther locule, in which the cytomictic channels connect each other of the cells [55]. This channel network may help the signalling for synchrony of male meiosis.

Is MEL2 required also for development of tapetal cells?

In addition to failure of meiotic entry, the *mel2* mutation caused the hypervacuolation and hypertrophy of tapetal cells (Figure 1I). This is different from the case of the maize *am1* mutant, in which no tapetal-cell degeneration has been reported [7,9]. Tapetal cells provide nutrients and pollen-wall materials to microspores, and degenerate, probably by PCD [56]. It is demonstrated that several gibberellin (GA)-related rice mutants display a hypertrophy of tapetal cells and result in male sterility [57]. This hypertrophic phenotype is attributed to the absence of PCD in the tapetum, because externally supplied GA can restore the tapetal phenotype of the *oscps1* mutation, which causes defects in GA biosynthesis. The hypertrophic tapetum in the GA-related mutations seems to resemble that in the *mel2* mutation. However, as opposed to GA mutants, apoptosis identified by the strong TUNEL signal arose in the *mel2* tapetum (Figure 1J). In addition, GA-related mutants can undergo meiosis and produce tetrad spores [57], distinct from the *mel2* mutant. These observations may suggest that *mel2*-dependent hypertrophy of the tapetum is independent of the GA-signalling pathway.

Both MEL2 mRNA and protein were expressed weakly in tapetal cells (Figure 2 and Figure 6). Thus, tapetal degeneration in *mel2* anthers would be a primary effect of the absence of MEL2 protein, while it is difficult to neglect the possibility that degeneration of PMCs directly causes tapetal-cell hypertrophy. MEL2 expression in tapetal cells appeared during early meiosis I (Figure 7). Tapetal cells are known to become multinucleate or polyploidized by mitoses without cytokinesis, in many cases during meiotic I prophase [58]. In rice, tapetal cells become binucleated, and in *Arabidopsis*, binucleation occurs synchronously at early leptotene. Thus, MEL2 function may be required not only for meiotic entry, but also for synchronous tapetal-cell binucleation, the disruption of which may induce hypertrophy and precocious tapetal-cell death. However, the synchronous expression of *H4* among tapetal cells was frequently observed even in *mel2* anthers (Figure 4H). It remains unclear whether this result excludes MEL2 function from the synchronization of tapetal-cell division.

In conclusion, we have proved that the RRM protein plays an essential role in plant germ-cell development in addition to yeast and metazoans, although the protein's structure, function, timing of expression, and subcellular localization differ between rice and non-plant species. This study also suggests that genome shuffling and the generation of a novel motif combination in ancestral monocots may have brought rice MEL2 a unique function in germline cell-cycle control. Further analysis of MEL2 function will contribute to better understanding of post-transcriptional or post-translational regulation of plant germ-cell development, and also to elucidating similarities and differences in reproduction systems between plants and other species.

Materials and Methods

Plant materials and genetic analysis

Seed-sterile mutant lines were selected as described [25]. For cytological and expression analyses, the F2 plants four-times backcrossed with cv. Nipponbare (BC4F2) were used. Non-transgenic plants were grown in a field in the city of Mishima, Shizuoka, Japan. Transgenic plants were grown in the growth chamber, LPH-2HCT (NK system), at 30°C for 14 hrs with the light and at 25°C for 10 hrs in dark.

The linkage relationship between the sterile phenotype and transposed *Tos17* fragments was analyzed by DNA gel blot hybridization and polymerase chain reaction (PCR) using the R3 population of 188 plants segregating the *mel2* seed-sterility. DNA extraction, DNA gel blotting, cloning and isolation of the *Tos17*-tagged genome sequence were performed as described [25]. PCR genotyping for the *mel2* mutant populations was performed using the mixture of three primers: 868, 869 and T17LTR4MF for *mel2-1* allele, or 870, 871 and T17LTR4MF for *mel2-2* allele (Table S1). 50- to 100-ng genomic DNAs and above three primers in 5-μL water were added to the same volume of GoTaq Green Master Mix (Promega).

Discrimination of developmental stages

The longitudinal length of flower buds and anthers was measured under the dissection microscopy SMZ645 (Nikon). The anther length is generally used as a criterion to determine developmental stages of germline cells in rice [59]. This criterion was also used in this study, because the anther length was increased proportional to longitudinal flower (or lemma) length, whose elongation was unaffected by *mel2* mutation, until the end of meiosis (Figure S12). A precise stage in each flower or anther was determined by the mRNA expression or immunofluorescence of stage-specific gene or protein markers.

Molecular cloning of *MEL2* cDNA

The full-length *MEL2* cDNA was obtained from 3.0-cm young rice panicles, frequently including flowers in premeiosis. RNA extraction and RACE reaction were according to the methods as described [26]. In addition to the oligo(dT)20 primer, two *MEL2* gene-specific, antisense primers, 871 and T2028R were used for three rounds of RTs, followed by the RACE-PCR with adaptor primers (AP1 and AP2) supplied by the manufacturer (Table S1). All products were cloned into pCR-BluntII-TOPO vector (Invitrogen), and sequenced by Dye Terminator Cycle Sequencing kit and ABI PRISM 3130xl Sequencer (Applied Biosystems). Three independent RACE fragments were combined into a single, full-length cDNA sequence by PCRs.

Complementation of sterile phenotype

The entire coding region of the *MEL2* gene and its 2.0-kbp upstream *cis*-sequence from the putative transcriptional start site were included within the 10-kbp of single *Sal*I genomic fragment (Figure S4). The 10-kbp fragment was isolated from the rice BAC clone OSJNBa0036A19, and subcloned into the pPZP2H-lac binary vector [60]. This plasmid or the empty vector as a negative control was introduced into *mel2-1* homozygous calli in accordance with the method as described [61]. The genotype of calli was determined by PCR, in which the template DNA was extracted from young shoots germinating on the callus-induction medium.

Analysis of *MEL2*-like gene

A sequence of the full length *MEL2* cDNA was supplied for the BLAST search on RAP-DB (http://rapdb.dna.affrc.go.jp/), and we found *Os12g0587100* locus (*MEL2like*) homologous to *MEL2* gene within rice genome. Genomic sequences of MEL2 coding region and *MEL2*-like locus were compared by HarrPlot program [62]. Specific primer sets for *MEL2*-like, TMEL2L1402F/TMEL2L1974R and 919/TMEL2L1974R were designed as referencing HarrPlot information and used for RT-PCR against the RNA extract from young flowers. Then we succeeded to amplify the *MEL2*-like transcript, in which the putative intron sequences were spliced out when compared with the genomic sequence.

Histology

Histological analysis of rice reproductive organs was done by using the plastic- embedded sections, the preparation method of which was described [25]. Sections were stained with toluidine blue (Chroma Gesellshaft Shaud) or provided for the TUNEL assay and other immunofluorescent analyses.

TUNEL was performed as described previously [56]. Plastic-embedded sections of rice panicles and flowers were treated with TUNEL apoptosis detection kit (DeadEnd Fluorometric TUNEL system, Promega) according to the manufacturer's instruction. The fluorescent TUNEL signal was detected by FV300 CLSM system and Photoshop.

Electron microscopic observation was done in accordance with the method described previously [39].

In situ hybridization

In situ hybridization against rice tissues was performed in accordance with the method as described [25]. To avoid a cross hybridization among highly homologous gene families, we adopted the high-stringency condition with 0.3 M NaCl and 50% formamide at 50°C for hybridization and 0.5xSSC at 50°C for wash. For the synthesis of RNA probes, two short ~500-bp DNA fragments were amplified by PCRs of the *MEL2* cDNA with the primer sets, 919/1034 and 1035/1036, respectively (Table S1). Both fragments were cloned into the pCRII-TOPO vector (dual promoter system) (Invitrogen), and transcribed to make antisense or sense RNA probes by SP6 or T7 promoters with DIG RNA labeling kit (Roche). Three PCR fragments against *OsCDKB2;1* cDNA were amplified by primer sets of M486F/M718R, M415F/M537R, and M609F/M739R, respectively, and cloned into pCRII-TOPO. The full-length 583-bp cDNA of rice histone *H4* (RAP-DB: Os09g0553100) was cloned into pBluescript SK- (Stratagene). Both plasmids were provided for the synthesis of RNA probes as in *MEL2*.

BrdU incorporation and detection

Fresh young panicles of 3–5 cm in length were curt from stems and placed in 100 µm BrdU solution in the dark for 4 hours. Plastic sectioning and detection of incorporated BrdU were done in accordance with the method described previously [39]. Before the immunization, ten minutes treatment of sections with Proteinase K (0.1 mg/mL, Sigma) often improved the accessibility of antibodies and the intensity of anti-T7-signals.

RT-PCR

To investigate the *MEL2* expression profile, total RNAs were extracted from various tissues of wild-type rice plants; embryo and endosperm from mature seeds, seedlings, shoot apices, leaf blades, leaf sheathes, roots, flag leaves, 1 cm young panicles, young flowers in 1–2 mm, 2–4 mm and 2–7 mm lengths, and mature flowers. All tissues were cut off and handled with forceps, and immediately transferred into microtubes filled with liquid nitrogen and stored at −80°C. RNeasy Plant Mini kit (QIAGEN) was used for RNA extraction. Total RNAs were reverse-transcribed with the oligo(dT)20 primer and SuperscriptIII reverse-transcriptase (Invitrogen), and provided for semi-quantitative RT-PCR. For *MEL2* mRNA, the primers, 918/919, were used. To investigate the structure of *MEL2* transcript in the *mel2* mutant, the primer sets, 918/919 and 868/869, were used. An expression of rice meiotic genes was examined in the *mel2* mutant flowers by using the following primer sets; 496/647 for *PAIR1*, 555/ 518 for *PAIR2*, and K180/K183 for *ZEP1*. The primer set ActinF/ActinR was used to amplify rice *Actin* cDNAs as a positive control.

Indirect immunofluorescence

Indirect immunofluorescent staining of rice meiocytes was performed in accordance with the method as described [39] with minor modifications. Rat anti-ZEP1 and rabbit anti-POT1 antibodies (Komeda, Kurata, and Nonomura, unpublished) were diluted in 1/1000 and 1/3000, respectively, and detected with AlexaFluor647 goat anti-rat IgG (Molecular Probes) and Cy3 goat anti-rabbit IgG (Amersham). Maximum four channels of fluorescent signals were simultaneously observed by Fluoview FV300 CLSM system, upgraded with LD405/440 laser unit (Olympus). Captured images were enhanced and pseudo-colored by Photoshop CS2 software (Adobe).

In vivo localization of recombinant T7 peptide-tagged MEL2

Plasmid constructions to produce T7 (MASMTGGQQMG)-tagged MEL2-expressing plants were based on the 10-kbp genomic *Sal*I-fragment same in the complementation test. The 10-kbp *Sal*I fragment (Figure S1) was subcloned into pT7Blue vector (Novagen). To add the T7 tag to the N-terminus of MEL2, the 476-bp fragment including the translational start site was amplified with the primers MEL2gApaI2F/MEL2gNotI2R, directly cloned into pCR-BluntII-TOPO vector (Invitrogen), and provided for site-directed insertion of T7-tag sequence by the inverted tail-to-tail direction PCR with primers MEL2T7NF/MEL2T7NR and for ligation as described [63]. This plasmid was again provided for PCR with MEL2gApaI2F/MEL2gNotI2R (476bp+T7). The *Apa*I-*Not*I fragment of MEL2g/pT7Blue plasmid was replaced to the 476bp+T7 fragment by In-Fusion Advantage PCR Cloning Kit (Clontech). Finally, the insert carrying the T7 tag was cut out with *Sal*I and inserted into *Sal*I site of the binary vector pPZP2H-lac [59]. To add the T7 tag to the C-terminus, the middle 4-kbp and the 3′-terminal 400-bp fragments of *MEL2* genome were amplified with primer sets, MEL2gSmaIF/MEL2InFu1R, and MEL2InFu1F/MEL2ctransEndR, respectively. The latter 400-bp fragment was cloned into pCR-BluntII-TOPO vector, and provided for site-directed insertion of T7-tag sequence just in front of *MEL2* stop codon (400bp+T7). The plasmid used for above complementation test was digested with *Sma*I to remove the latter half 5.5-kbp genomic fragment. The rest sequence, including pPZP2H-lac and the first half of *MEL2* gene, was fused with the middle 4-kbp and the 400bp+T7 fragments by In-Fusion Cloning Kit. Two resultant binary plasmids, the N-tagged MEL2 plasmid (MEL2gT7N/pPZP2H-lac) and the C-tagged one (MEL2gT7C/pPZP2H-lac), were introduced into *mel2*/*mel2* calli, and transgenic plants were regenerated according to the method as described [60].

Immunocytology was done by using plastic sections of transgenic anthers in accordance with indirect immunofluores-

cense above mentioned, with goat anti-T7 antibody (Bethyl Laboratory) as a primary antibody and AlexaFluor488 donkey anti-goat IgG (Molecular Probes) for detection.

Supporting Information

Figure S1 The *mel2* seed-sterile phenotype was attributed to the complete elimination of male and female gametogenesis. (A) The *mel2* mutant set no seed at the harvest stage, though the vegetative growth was not affected by the mutation. (B, C) The longitudinal, optical sections of an anther lobe at the flowering stage in the wild-type (B) and *mel2-1* mutant (C). The mutant anther failed to produce mature pollens. (D, E) The longitudinal, optical sections of an ovule at the flowering stage in the wild-type (D) and *mel2-1* mutant (E). The mature embryo-sac was completely eliminated in the mutant.
Found at: doi:10.1371/journal.pgen.1001265.s001 (0.34 MB TIF)

Figure S2 The size of pollen mother cells (PMCs) became various in *mel2* mutant anthers. (A) PMCs in various sizes were observed at early meiosis I in the mutant anther (right), whereas an equational size of PMCs was in the wild-type anther (left). In mutant anthers, meiotic chromosome condensation was scarcely observed, even though the anther was grown enough to enter meiosis. The mutant PMCs frequently contained the smaller nucleus (red arrows) comparable to the somatic nuclei (yellow arrowheads). In addition, a few PMCs underwent mitotic cell division (red arrowheads). Bars, 20 μm. (B) The PMC size became varied and smaller in the *mel2* mutant than in the wild type. In the histogram, the size was represented by the area of PMCs optically sectioned, binarized on the software ImageJ ver.1.41, and normalized with the averaged area of soma cells. The relative value of the averaged PMC area was 2.27 ± 0.30 in the wild type, and 2.07 ± 0.58 in the mutant.
Found at: doi:10.1371/journal.pgen.1001265.s002 (0.20 MB TIF)

Figure S3 The ultrastructure of pollen mother cells (PMCs) at early meiosis I. (A) A cross section of the wild-type anther. Nu, nucleus; Ca, callose wall; Ta, tapetal cell. (B) A magnified view of the squared region in (A). Mi, mitochondrion. (C) A cross section of the *mel2* mutant anther. V, vacuole. (D) A magnified view of the squared region in (C). Mm, megamitochondrion. Bars, 2 μm in (A, C) and 0.1 μm in (B, D).
Found at: doi:10.1371/journal.pgen.1001265.s003 (1.64 MB TIF)

Figure S4 The 10-kbp genomic *Sal*I-fragment assigned by the locus *Os12g0572800* includes the functional *MEL2* gene. (A) Segregants of the seed-sterile line ND00278 were provided for Southern blot analysis. In the left panel, using the partial sequence of *Tos17* (Nonomura et al. 2003) as a probe, ten or more bands of XbaI-DNA fragments were detected. f, fertile; S, sterile; m, marker. An appearance of the band pointed by a large arrow indicates the *Tos17* insertion completely linked with the sterility. Small arrows show the original two *Tos17* copies in the rice variety cv. Nipponbare. In the right panel, using the *Tos17*-flanking sequence of the locus *Os12g0572800* , the genotype homo- or heterozygous for *Tos17* insertion was clearly distinguishable, and the complete linkage between the insertion and the sterility was reproducible. A closed arrowhead and an arrow indicate the allelic bands with and without the *Tos17* insertion, respectively. The bands pointed by an open arrowhead were derived from the *MEL2*-like locus *Os12g0587100*. (B) The *Sal*I-fragment including the entire *MEL2* gene composed of 14 exons. Each *Tos17* insertion site of *mel2-1* or *mel2-2* allele was indicated within the seventh or twelfth exon, respectively. The arrowheads indicate three antisense primers used for three rounds of 5′-RACE. (C) The transgenic *mel2/mel2* plants carrying the 10-kbp *Sal*I-fragment recovered the fertility. but sibling plants without the fragment became sterile.
Found at: doi:10.1371/journal.pgen.1001265.s004 (0.09 MB TIF)

Figure S5 An amino-acid sequence of MEL2 protein deduced from the cDNA sequence. The mylistoylation motif at the N-terminal end was enclosed by the open box. The ten imperfect ankyrin repeats were colored in red, and the consensus peptides were underlined. The RNA recognition motif was colored in blue. The proline (P) was bolded, and the P-rich region was wavy-underlined. The nonary repeats within the P-rich region were shown by shadow boxes. The RING finger motif was colored in green, and the consensus cystein and histidine residue were double-underlined.
Found at: doi:10.1371/journal.pgen.1001265.s005 (0.20 MB TIF)

Figure S6 The alignment of MEL2 proteins of rice, *Sorgham* and *Brachypodium*. The conserved residues were highlighted. The ankyrin repeats were underlined with wavy lines. RNP1 and RNP2 were underlined, and the RING finger motif was double-underlined.
Found at: doi:10.1371/journal.pgen.1001265.s006 (0.36 MB TIF)

Figure S7 The *MEL2*-like genomic sequence would become a pseudo-gene. (A) The position and orientation of *MEL2* (*Os12g0572800*) and *MEL2*-like (*Os12g0587100*) loci on the rice chromosome 12. (B) HarrPlot comparison between genomic sequences of *MEL2* and *MEL2*-like genes. The points at which eight or more basepairs were sequentially identical between *MEL2* and *MEL2*-like sequences were dotted in this graph. The arrowheads which face each other indicate the position of primers used in the RT-PCR of *MEL2*-like gene. (C) Alignment of the *MEL2* and *MEL2*-like cDNA sequences, involving the middle region of the *MEL2* cDNA which encodes two RRM motifs and the nuclear localization signal. The underlined sequences indicate primers shown in the panel B (arrowheads). The asterisks indicate identical nucleotides between both cDNAs. The asterisk and box colored in red shows one-basepair insertion found in *MEL2*-like cDNA.
Found at: doi:10.1371/journal.pgen.1001265.s007 (0.41 MB TIF)

Figure S8 The results of reverse transcriptase-polymerase chain reactions (RT-PCRs). (A) *MEL2* and *MEL2*-like genes were expressed in young flowers. The *MEL2* signal was observed also in the leaf blade and sheath. In the middle panel, the arrow indicates the band from the *MEL2*-like mRNA. (B, C) In situ hybridization of the *MEL2* antisense (B) and sense (C) probes against the cross-sections from the wild-type stem. The lb and ls indicate the leaf blade and sheath, respectively. Both reactions gave no difference, indicating that the expression in leaves in (A) should be under the detection level in in situ hybridization. (D) RT-PCR revealed that rice meiotic genes *PAIR1*, *PAIR2* and *ZEP1* are expressed normally even in the *mel2* mutant flowers.
Found at: doi:10.1371/journal.pgen.1001265.s008 (0.13 MB TIF)

Figure S9 An aberrant form of the *MEL2* mRNA was expressed in the *mel2* mutant flowers. Using the primer set p919/p918, which target the C-terminal region including the RING finger motif, the predicted wild-type size of PCR fragment was amplified in both the wild-type (+/+) and the *mel2* mutant flowers (−/−). (A). Using the primer set p868/p869, however, the *Tos17*-inserted fragment was only amplified in the *mel2* mutant (B), whereas the smaller wild-type size was amplified in the wild type (C). *OsACT* is the RT-PCR of rice *Actin* genes as a positive control.
Found at: doi:10.1371/journal.pgen.1001265.s009 (0.08 MB TIF)

Figure S10 A typical meiotic arrangement of centromeres and telomeres was hardly observed at early prophase I in *mel2*

meiocytes. Chromosomes were counter-stained with DAPI (blue). (A) The wild-type meiocyte nucleus at early zygotene. A telomere binding protein OsPOT1 (green) associated with the nuclear envelop and made a cluster at the restricted portion (an arrowheads), so-called bouquet structure. In contrast, OsCenH3 (magenta), the rice homolog of human CenpA, located at the nuclear interior, and formed chromocenters. (B) The *mel2* meiocyte nucleus at early zygotene. In contrast to the wild type, centromeres associated with the nuclear envelope and telomeres located at the nuclear interior, which was a typical arrangement of premeiotic meiocytes or soma (C). Bars, 5 μm.
Found at: doi:10.1371/journal.pgen.1001265.s010 (0.18 MB TIF)

Figure S11 T7-tagged *MEL2* transgenes rescued the seed-sterile phenotype of the *mel2* mutant. (A) The PCR genotyping of the self-pollinated first generation of transgenic plants (T1 plants) carrying T7-tagged *MEL2* transgenes. V, C and N indicates that the T0 plant is transformed with the empty vector, the C- and N-tagged *MEL2* transgene, respectively. The C- and N-tagged constructs were introduced into the homozygous mel2-1/mel2-1 mutant plants, whereas the empty vector was into the heterozygous *MEL2/mel2-1* plants. In each V2, C9 or N6 plant, #1 to #3 indicates that these T1 plants are the sibling. The PCR primers for the genotyping of the *mel2-1* mutant (see Supplemental methods) were used for the genotyping of transgenic plants here. This PCR amplified two fragments; from the wild-type (upper) and the mutated (lower) *MEL2* sequences. All lower fragments arose from the mutant *mel2-1* allele. In the V2#1 and #2, the upper fragment arose from the wild-type *MEL2* allele, whereas in the C9 and N6 plants the upper from the wild-type *MEL2* transgene. (B) The seed fertility of the T1 transgenic plants in (A). All plants emanating the upper band in (A) restored the sterile phenotype of the *mel2* mutant, indicating that the T7-tagged *MEL2*constructs were functional *in vivo*.
Found at: doi:10.1371/journal.pgen.1001265.s011 (0.07 MB TIF)

Figure S12 The elongation of spikelet (lemma) length was proportional to the elongation of anther length in both the wild type (open circulars) and the *mel2* mutant (closed square).
Found at: doi:10.1371/journal.pgen.1001265.s012 (0.03 MB TIF)

Table S1 Summary table listing PCR primers used in this study.
Found at: doi:10.1371/journal.pgen.1001265.s013 (0.06 MB DOC)

Acknowledgments

We thank M. Umeda (NAIST, Japan) and S. Toki (NIAS, Japan) for kindly providing the information of OsCDKB2;1 and useful discussions, and we thank S. Saeki and K. Kondo (NIG) for devoted assistance on field works.

Author Contributions

Conceived and designed the experiments: KI Nonomura, N Kurata. Performed the experiments: KI Nonomura, M Eiguchi, M Nakano, K Takashima, S Miayzaki. Analyzed the data: S Fukuchi. Contributed reagents/materials/analysis tools: N Komeda, A Miyao, H Hirochika. Wrote the paper: KI Nonomura.

References

1. Pawlowski WP, Sheehan MJ, Ronceret A (2007) In the beginning: the initiation of meiosis. BioEssays 29: 511–514.
2. Ito M, Takegami MH (1982) Commitment of mitotic cells to meiosis during the G2 phase of premeiosis. Plant Cell Physiol 23: 943–952.
3. Hamant O, Ma H, Cande WZ (2006) Genetics of meiotic prophase I in plants. Annu Rev Plant Biol 57: 267–302.
4. Mercier R, Vezon D, Bullier E, Motamayor JC, Sellier A, et al. (2001) SWITCH1 (SWI1): a novel protein required for the establishment of sister chromatid cohesion and for bivalent formation at meiosis. Genes Dev 15: 1859–1871.
5. Agashe B, Prasad CK, Siddiqi I (2002) Identification and analysis of DYAD: a gene required for meiotic chromosome organisation and female meiotic progression in *Arabidopsis*. Development 129: 3935–3943.
6. Pawlowski WP, Wang CJ, Golubovskaya IN, Szymaniak JM, Shi L, et al. (2009) Maize AMEIOTIC1 is essential for multiple early meiotic processes and likely required for the initiation of meiosis. Proc Natl Acad Sci USA 106: 3603–3608.
7. Palmer RG (1971) Cytological studies of ameiotic and normal maize with reference to premeiotic pairing. Chromosoma 35: 233–246.
8. Staiger CJ, Cande WZ (1992) Ameiotic, a gene that controls meiotic chromosome and cytoskeletal behavior in maize. Dev Biol 154: 226–230.
9. Golubovskaya I, Grebennikova ZK, Avalkina NA, Sheridan WF (1993) The role of the *ameiotic1* gene in the initiation of meiosis and in subsequent meiotic events in maize. Genetics 135: 1151–1166.
10. Schmitz RJ, Amasino RM (2007) Vernalization: a model for investigating epigenetics and eukaryotic gene regulation in plants. Biochim Biophys Acta 1769: 269–275.
11. Armstrong SJ, Franklin FCH, Jones GH (2003) A meiotic time-course for *Arabidopsis thaliana*. Sex Plant Reprod 16: 141–149.
12. Nonomura KI, Nakano M, Murata K, Miyoshi K, Eiguchi M, et al. (2004) An insertional mutation in the rice *PAIR2* gene, the ortholog of *Arabidopsis ASY1*, results in a defect in homologous chromosome pairing during meiosis. Mol Gen Genomics 271: 121–129.
13. Magnard JL, Yang M, Chen YC, Leary M, McCormick S (2001) The *Arabidopsis* gene *tardy asynchronous meiosis* is required for the normal pace and synchrony of cell division during male meiosis. Plant Physiol 127: 1157–1166.
14. Wang Y, Magnard JL, McCormick S, Yang M (2004) Progression through meiosis I and meiosis II in *Arabidopsis* anthers is regulated by an A-type cyclin predominately expressed in prophase I. Plant Physiol 136: 4127–4135.
15. Siomi H, Dreyfuss G (1997) RNA-binding proteins as regulators of gene expression. Curr Opin Genet Dev 7: 345–353.
16. Harigaya Y, Tanaka H, Yamanaka S, Tanaka K, Watanabe Y, et al. (2006) Selective elimination of messenger RNA prevents an incidence of untimely meiosis. Nature 442: 45–50.
17. Carani C, Gromoll J, Brinkworth MH, Simoni M, Weinbauer GF, et al. (1997) *cynDAZLA*: a cynomolgus monkey homologue of the human autosomal *DAZ* gene. Mol Hum Reprod 3: 479–483.
18. Maines JZ, Wasserman SA (1999) Post-transcriptional regulation of the meiotic Cdc25 protein Twine by the Dazl orthologue Boule. Nat Cell Biol 1: 171–174.
19. Karashima T, Sugimoto A, Yamamoto M (2000) *Caenorhabditis elegans* homologue of the human azoospermia factor *DAZ* is required for oogenesis but not for spermatogenesis. Development 127: 1069–1079.
20. Chen CY, Shyu AB (1995) AU-rich elements: characterization and importance in mRNA degradation. Trends Biochem Sci 20: 465–470.
21. Collier B, Gorgoni B, Loveridge C, Cooke HJ, Gray NK (2005) The DAZL family proteins are PABP-binding proteins that regulate translation in germ cells. EMBO J 24: 2656–2666.
22. Reynolds N, Collier B, Bingham V, Gray NK, Cooke HJ (2007) Translation of the synaptonemal complex component Sycp3 is enhanced in vivo by the germ cell specific regulator Dazl. RNA 13: 974–981.
23. Kaur J, Sebastian J, Siddiqi I (2006) The *Arabidopsis-mei2-like* genes play a role in meiosis and vegetative growth in *Arabidopsis*. Plant Cell 18: 545–559.
24. Tsui S, Dai T, Roettger S, Schempp W, Salido EC, et al. (2000) Identification of two novel proteins that interact with germ-cell-specific RNA-binding proteins DAZ and DAZL1. Genomics 65: 266–273.
25. Nonomura KI, Miyoshi K, Eiguchi M, Suzuki T, Miyao A, et al. (2003) The *MSP1* gene is necessary to restrict the number of cells entering into male and female sporogenesis and to initiate anther wall formation in rice. Plant Cell 15: 1728–1739.
26. Nonomura KI, Morohoshi A, Nakano M, Eiguchi M, Miyao A, et al. (2007) A germ cell specific gene of the *ARGONAUTE* family is essential for the progression of premeiotic mitosis and meiosis during sporogenesis in rice. Plant Cell 19: 2583–2594.
27. Chen R, Zhao X, Shao Z, Wei Z, Wang Y, et al. (2007) Rice UDP-glucose pyrophosphorylase1 is essential for pollen callose deposition and its cosuppression results in a new type of thermosensitive genic male sterility. Plant Cell 19: 847–861.
28. Karbowski, M, CKurono, MWozniak, MOstrowski, MTeranishi, Y, et al. (1999) Free radical-induced megamitochondria formation and apoptosis. Free Radic Biol Med 26: 396–409.
29. Resh MD (1999) Fatty acylation of proteins: new insights into membrane targeting of myristoylated and palmitoylated proteins. Biochim Biophys Acta 1451: 1–16.
30. Sedgwick SG, Smerdon SJ (1999) The ankyrin repeat: a diversity of interactions on a common structural framework. Trends Biochem Sci 24: 311–316.
31. Kenan DJ, Query CC, Keene JD (1991) RNA recognition: towards identifying determinants of specificity. Trends Biochem Sci 16: 214–220.

32. Birney E, Kumar S, Krainer AR (1993) Analysis of the RNA-recognition motif and RS and RGG domains: conservation in metazoan pre-mRNA splicing factors. Nucleic Acids Res 21: 5803–5816.
33. Burd CG, Dreyfuss G (1994) RNA binding specificity of hnRNP A1: significance of hnRNP A1 high-affinity binding sites in pre-mRNA splicing. EMBO J 13: 1197–1204.
34. Altschul SF, Madden TL, Schaffer AA, Zhang J, Zhang Z, et al. (1997) Gapped BLAST and PSI-BLAST: a new generation of protein database search programs. Nucleic Acids Res 25: 3389–3402.
35. Kawabata T, Fukuchi S, Homma K, Ota M, Araki J, et al. (2002) GTOP: a database of protein structures predicted from genome sequences. Nucleic Acids Res 30: 294–298.
36. Fukuchi S, Homma K, Sakamoto S, Sugawara H, Tateno Y, et al. (2009) The GTOP database in 2009: updated content and novel features to expand and deepen insights into protein structures and functions. Nucleic Acids Res (Database issue) 37: D333–337.
37. Umeda M, Umeda-Hara C, Yamaguchi M, Hashimoto J, Uchimiya H (1999) Differential expression of genes for cyclin-dependent protein kinases in rice plants. Plant Physiol 119: 31–40.
38. Bass HW, Marshall WF, Sedat JW, Agard DA, Cande WZ (1997) Telomeres cluster *de novo* before the initiation of synapsis: a three-dimensional spatial analysis of telomere positions before and during meiotic prophase. J Cell Biol 137: 5–18.
39. Nonomura KI, Nakano M, Eiguchi M, Suzuki T, Kurata N (2006) PAIR2 is essential for homologous chromosome synapsis in rice meiosis I. J Cell Sci 119: 217–225.
40. Wang M, Wang K, Tang D, Wei C, Li M, et al. (2010) The Central Element Protein ZEP1 of the Synaptonemal Complex Regulates the Number of Crossovers during Meiosis in Rice. Plant Cell, tpc.109.070789.
41. Podell S, Gribskov M (2004) Predicting N-terminal myristoylation sites in plant proteins. BMC Genomics 5: 37.
42. Li XC, Barringer BC, Barbash DA (2009) The pachytene checkpoint and its relationship to evolutionary patterns of polyploidization and hybrid sterility. Heredity 102: 24–30.
43. Caryl AP, Jones GH, Franklin FC (2003) Dissecting plant meiosis using *Arabidopsis thaliana* mutants. J Exp Bot 54: 25–38.
44. Dreyfuss G, Matunis MJ, Pinol-Roma S, Burd CG (1993) hnRNP proteins and the biogenesis of mRNA. Annu Rev Biochem 62: 289–321.
45. Vera Y, Dai T, Hikim AP, Lue Y, Salido EC, et al. (2002) Deleted in azoospermia associated protein 1 shuttles between nucleus and cytoplasm during normal germ cell maturation. J Androl 23: 622–628.
46. Lin YT, Yen PH (2006) A novel nucleocytoplasmic shuttling sequence of DAZAP1, a testis-abundant RNA-binding protein. RNA 12: 1486–1493.
47. Kurihara Y, Watanabe H, Kawaguchi A, Hori T, Mishiro K, et al. (2004) Dynamic changes in intranuclear and subcellular localizations of mouse Prrp/DAZAP1 during spermatogenesis: the necessity of the C-terminal proline-rich region for nuclear import and localization. Arch Histol Cytol 67: 325–333.
48. Hsu LC, Chen HY, Lin YW, Chu WC, Lin MJ, et al. (2008) DAZAP1, an hnRNP protein, is required for normal growth and spermatogenesis in mice. RNA 14: 1814–1822.
49. Moore FL, Jaruzelska J, Fox MS, Urano J, Firpo MT, et al. (2003) Human Pumilio-2 is expressed in embryonic stem cells and germ cells and interacts with DAZ (Deleted in AZoospermia) and DAZ-like proteins. Proc Natl Acad Sci USA 100: 538–543.
50. Urano J, Fox MS, Reijo Pera RA (2005) Interaction of the conserved meiotic regulators, BOULE (BOL) and PUMILIO-2 (PUM2). Mol Reprod Dev 71: 290–298.
51. Kreft SG, Nassal M (2003) hRUL138, a novel human RNA-binding RING-H2 ubiquitin-protein ligase. J Cell Sci 116: 605–616.
52. Nodzon LA, Xu WH, Wang Y, Pi LY, Chakrabarty PK, et al. (2004) The ubiquitin ligase XBAT32 regulates lateral root development in Arabidopsis. Plant J 40: 996–1006.
53. Prasad ME, Schofield A, Lyzenga W, Liu H, Stone SL (2010) *Arabidopsis* RING E3 ligase XBAT32 Regulates Lateral Root Production through its Role in Ethylene Biosynthesis. Plant Physiol;DOI:10.1104/pp.110.156976.
54. Wolfe KH, Gouy M, Yang YW, Sharp PM, Li WH (1989) Date of the monocot-dicot divergence estimated from chloroplast DNA sequence data. Proc Natl Acad Sci USA 86: 6201–6205.
55. Heslop-Harrison J (1966) Cytoplasmic connexions between angiosperm meiocytes. Annals Bot 30: 221–230.
56. Li N, Zhang DS, Liu HS, Yin CS, Li XX, et al. (2006) The rice tapetum degeneration retardation gene is required for tapetum degradation and anther development. Plant Cell 18: 2999–3014.
57. Aya K, Ueguchi-Tanaka M, Kondo M, Hamada K, Yano K, et al. (2009) Gibberellin modulates anther development in rice via the transcriptional regulation of GAMYB. Plant Cell 21: 1453–1472.
58. Weiss H, Maluszynska J (2001) Molecular cytogenetic analysis of polyploidization in the anther tapetum of diploid and autotetraploid *Arabidopsis thaliana*. Annals Botany 87: 729–735.
59. Itoh J, Nonomura KI, Ikeda K, Yamaki S, Inukai Y, et al. (2005) Rice plant development: from zygote to spikelet. Plant Cell Physiol 46: 23–47.
60. Fuse T, Sasaki T, Yano M (2001) Ti-plasmid vectors useful for functional analysis of rice genes. Plant Biotech 18: 219–222.
61. Hiei Y, Ohta S, Komari T, Kumashiro T (1994) Efficient transformation of rice (*Oryza sativa* L.) mediated by *Agrobacterium* and sequence analysis of the boundaries of the T-DNA. Plant J 6: 271–282.
62. Staden R (1982) An interactive graphics program for comparing and aligning nucleic acid and amino acid sequences. Nucleic Acids Res 10: 2951–2961.
63. Imai Y, Matsushima Y, Sugimura T, Terada M (1991) A simple and rapid method for generating a deletion by PCR. Nucleic Acids Res 19: 2785.